FUSED FILAMENT FABRICATION 3D PRINTING OF CONTINUOUS CARBON FIBER REINFORCED THERMOPLASTIC: RELATION BETWEEN CROSS-POINTS DISTRIBUTION AND TENSILE PERFORMANCE

Gongshuo Wang[1], Fuji Wang[1*], Shouyan Guan[1], Hongquan Wang[1], Jianming Zhou[1] and Rao Fu[1]

[1] School of Mechanical Engineering, Dalian University of Technology, Dalian, China, 116024
Email: wgs1016@mail.dlut.edu.cn (G. Wang), wfjsll@dlut.edu.cn (F. Wang),
guansy@mail.dlut.edu.cn (S. Guan), whq@mail.dlut.edu.cn (H. Wang),
zhoujianming@mail.dlut.edn.cn (J. Zhou), r.fu@dlut.edu.cn (R. Fu),
Webpage: http://faculty.dlut.edu.cn/2005011097/zh_CN/index.htm (F. Wang),
http://faculty.dlut.edu.cn/furao/zh_CN/index.htm (R. Fu).

Keywords: 3D printing, CFRTP, Cross-points distribution, Trajectory planning, Tensile performance

ABSTRACT

Continuous carbon fiber reinforced thermoplastic composites (C-CFRTP) have been widely used in high-end equipment with the development of injection molding and compression molding technologies, owing to their excellent mechanical properties and integrated manufacturing feasibility. Recently, fused filament fabrication (FFF) 3D printing technology of C-CFRTP has become a new fabrication method especially for parts with complex structures, of which load-bearing has been significantly improved due to the application of the constant continuous carbon fiber. Trajectory planning is the key process to ensure that the fiber remains continuous at all time, and has been a hotspot in the academic field. Double-curve connection trajectory has been proposed by the authors to keep the fiber continuous during the printing process, and this paper has further investigated the effects of the cross-points distribution, a key processing parameter of this process, on the tensile performance. The cross-points were classified as intra-layer cross-points and inter-layer cross-points, and the fracture modes of C-CFRTP parts with different cross-points distributions were analysed. As the cross-points distribution varied, the fracture mode of parts printed by double-curve connection trajectory gradually changed from mode 1 (all cross-points failure) to mode 3 (only one cross-point failure), and the tensile strength of those parts increased at the same time. The relation between cross-points distribution and tensile performance has been built and experimentally validated. Based on this relation, the cross-points distribution was optimized for obtaining higher tensile strength. Compared with the parts printed by the unoptimized cross-points distribution trajectory, the tensile strength of the parts printed by the optimized cross-points distribution trajectory was improved by about 19.97%. In addition, a further comparison between the proposed trajectory and the Zig-Zag trajectory, not usually used for parts with complex structures, has been investigated and the results showed a very close tensile strength, which also demonstrated the advantages of double-curve connection trajectory. The findings in this paper could promote the development of 3D printing C-CFRTP trajectory planning and improve the mechanical performance of parts with complex structures.

1 INTRODUCTION

Continuous carbon fiber reinforced thermoplastic composites (C-CFRTP) have been broadly used in the field of high-end equipment manufacturing due to its outstanding material properties such as high strength-to-weight ratio, excellent corrosion resistance, low coefficient of thermal expansion, and recyclability [1, 2]. Limited by the high cost of mold and the manufacturing boundedness of complex structures, traditional methods for C-CFRTP manufacturing, such as injection molding, compression molding, etc., inevitably encounter bottlenecks in manufacturing the parts with complex structures [3]. Fused filament fabrication (FFF), the most widely used 3D printing technology, has rapidly developed in recent years. Thanks to the layer-by-layer material build-up approach, the FFF 3D printing technology provides a new method to fabricate C-CFRTP parts with complex structures [4].

The FFF 3D printing of C-CFRTP has been investigated to produce advanced composite parts with complex structures. Mark one, the first 3D printer of C-CFRTP, was unveiled in 2014, which adopted the towpreg extrusion process to fabricate C-CFRTP parts [5]. Meanwhile, the 3D printer that employed the FFF technology of the in-suit impregnation process has been proposed by Tian et al. [6]. Based on those two types of 3D printers, researchers have investigated the effect of process parameter optimization [7], fiber surface pretreatment [8], and auxiliary processes [9] on the mechanical performance of FFF-fabricated C-CFRTP parts. Although those studies have greatly improved the performance of FFF-fabricated C-CFRTP parts, there was still a gap compared to those manufactured by traditional methods.

Trajectory planning, as the vital preparation step before 3D printing, significantly impacted on the performance of FFF-fabricated parts [10]. Especially for C-CFRTP, the printing trajectory directly determined the fiber-laydown pattern, which was the key factor affecting the part's performance. Therefore, great efforts have been attempted to explore a suitable printing trajectory so that the performance of FFF-fabricated parts can be improved further. Initially, two types of printing trajectory were applied for FFF 3D printing C-CFRTP, including Zig-Zag trajectory [11, 12] and offset trajectory [13]. In order to determine the printing trajectory that can fabricate the part with better mechanical properties, Andrew et al. [14] compared the mechanical performance of C-CFRTP parts printed by those two trajectories. The results indicated that the parts printed by the Zig-Zag trajectory exhibited better tensile performance, while those printed by the contour offset trajectory performed better flexural performance. Based on that, the complex structural parts, such as honeycomb sandwich [15], lattice truss [16], specimens with drilled holes [17], and Messerschmitt-Bölkow-Blohm (MBB) beam [18], have been printed by the special trajectory. Due to the limitations of complex structures, there are jumping points in the printing trajectory. The jumping points make the fiber discontinuity, leading to premature failure of the part in the area where the fiber is discontinuous [19]. To solve this problem, the double-curve connection trajectory was proposed [20]. This trajectory built the special "bridges" between adjacent trajectories to avoid jumping points. The results showed that the tensile strength of the C-CFRTP part printed by double-curve connection trajectory was greater than that of the part printed by the offset trajectory while less than that of the part printed by the Zig-Zag trajectory (non-cross-points trajectory). The cross-points ("bridges") in the double-curve connection trajectory decreased the tensile performance of the C-CFRTP part. Fortunately, the double-curve connection trajectory allows for a reasonable cross-points distribution, which can reduce the impact of cross-points on the tensile performance of parts. However, the unrevealed relation between cross-points distribution and tensile performance makes it impossible to provide a basis for distributing cross-points, which affects the performance improvement of the C-CFRTP part printed by double-curve connection trajectory.

For this purpose, the influence of cross-points distribution on tensile performance was investigated in this paper. Based on the fracture mode of the C-CFRTP part printed by double-curve connection trajectory, the relation between cross-points distribution and tensile performance was built through theoretical analysis. Then the relation was verified by measuring the tensile strength of parts printed by double-curve connection trajectory with different cross-points distributions. After that, the cross-points distribution was optimized, which made the tensile strength of parts printed by double-curve connection trajectory close to that of parts printed by the Zig-Zag trajectory. The findings in this paper could promote the application of double-curve connection trajectory and improve the mechanical performance of FFF-fabricated C-CFRTP parts.

2 RELATION BETWEEN CROSS-POINTS DISTRIBUTION AND TENSILE PREFORMANCE

2.1 Model simplification of specimens printed by double-curve connection trajectory

According to the double-curve connection trajectory planning method, two adjacent fiber bundles will cross each other to form the cross-point, as shown in Figure 1(a). For the convenience of graphic indication, the schematic of Figure 1(b) was used to represent the cross-point between two adjacent fiber bundles. In the double-curve connection trajectory schematic, a straight line with a solid circle represents two adjacent fiber bundles crossing each other, and the solid circle represents the cross-point. Besides, limited by the double-curve connection trajectory planning method, there are two fiber bundles within the same layer which do not intersect with any fiber bundles. A straight line without solid circle represents the fiber bundle that does not intersect with other fiber bundles in the schematic. The position relationship between cross-points determined the types of cross-points. As shown in Figure 1(b), cross-points in the same printing plane are recorded as the intra-layer cross-points, while cross-points in the same Z-directional plane are marked as inter-layer cross-points.

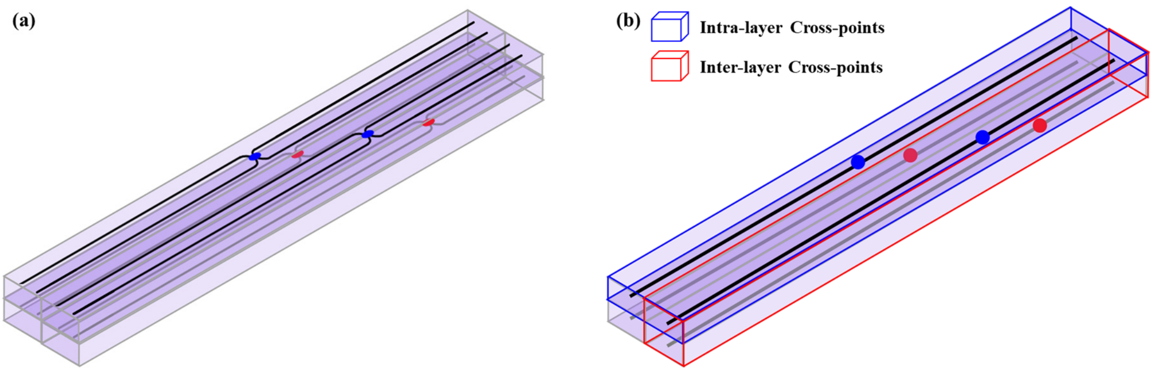

Figure 1: The schematic of double-curve connection trajectory. (a) The double-curve connection trajectory and (b) the simplified diagram of double-curve connection trajectory.

As shown in Figure 2(a), d represents the distance between two adjacent cross-points along the fiber direction, and d_0 represents the length of the cross-point area along the fiber direction. During the load-bearing process, the continuous fiber bundle bears tensile stress, while the matrix between the continuous fiber bundle bears shear stress. As shown in Figure 2(b), σ_x and σ_c represent the tensile strength of fiber bundles with non-cross-points and the tensile strength of fiber bundles at cross-points, respectively. τ indicates the shear strength of the matrix between two cross-points. The fiber orientation at cross-points is inconsistent with the direction of the external load, resulting in a weak bearing capacity in cross-points, namely $\sigma_x > \sigma_c$. Since the cross-point area possesses a certain length in the fiber direction, tiny pores will be between the cross-points and the adjacent fiber bundles. The load between the fiber bundles cannot be transferred in this area.

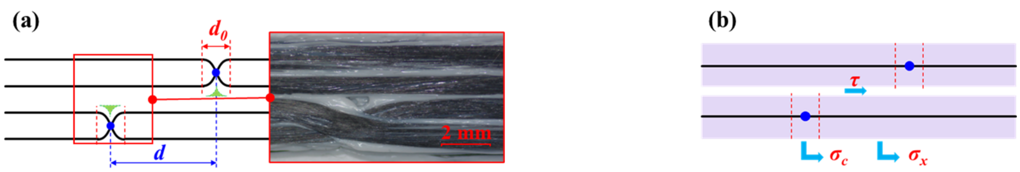

Figure 2: (a) the geometric parameters of cross-points and (b) internal stress of C-CFRTP parts during the load-bearing process.

2.2 Fracture modes analysis of specimens

When $d \leq d_0$, the pores of the adjacent two cross-points are almost connected, as shown in Figure 3(a). The connected pores at the adjacent cross-points lead to the concentration of the weak load-bearing capacity for the C-CFRTP part. In this case, all the cross-points will fail under the action of tensile loads, resulting in the fracture mode 1, as shown in Figure 3(a). When $d > d_0$, the pores of the adjacent two cross-points are separated, which allows the matrix between adjacent fiber bundles to transmit shear loads. In this case, the prerequisite for C-CFRTP part fracture is the simultaneous failure of all cross-points and the matrix between adjacent cross-points, as shown in Figure 3(b). As d increases, there is almost no mutual influence between adjacent cross-points, resulting in the part breaking flush perpendicular to the fiber bundles direction at a certain cross-point, as shown in Figure 3(c).

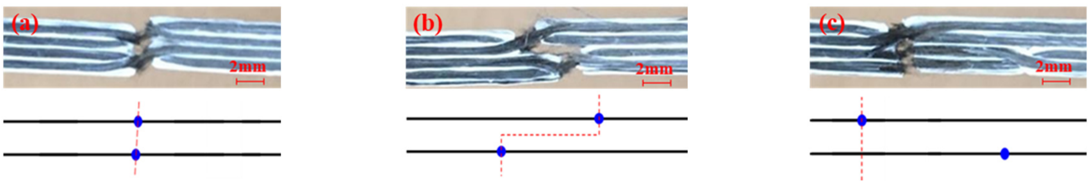

Figure 3: The fracture mode of C-CFRTP parts printed by double-curve connection trajectory: (a) Mode 1: all cross-points fail, (b) Mode 2: all cross-points and the shear planes among them fail, and (c) Mode 3: one cross-point and straight fiber on the same section fail.

2.3 Relation development

Cross-points in the double-curve connection trajectory can be classified into intra-layer and inter-layer cross-points. Based on that, the relation between cross-points distribution and tensile performance was built in this section. Moreover, it is assumed that the cross-points are uniformly distributed along the fiber direction to facilitate building this relation.

As shown in Figure 4(a), there are n cross-points in the single-layer 3D-printed C-CFRTP part with the length of L and the width of W. The width of a single fiber bundle is b, and the height of that is h. With the distance between the adjacent intra-layer cross-points (d_p) gradually increasing, the C-CFRTP part will fail in different fracture modes, leading to the change in tensile strength.

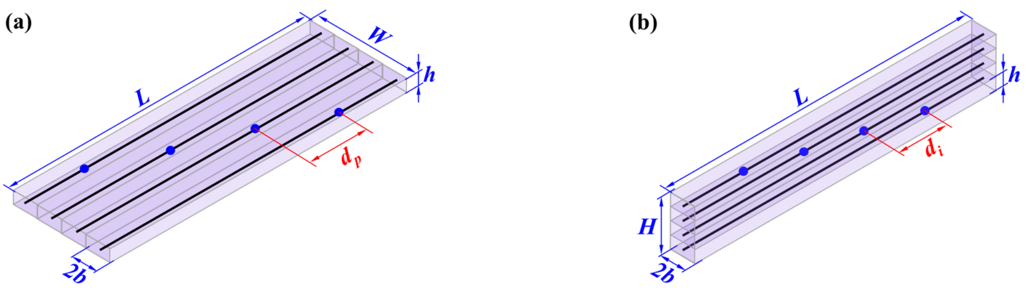

Figure 4: The distribution of (a) intra-layer cross-points in the same printing plane and (b) inter-layer cross-points in the same Z-directional plane.

When $d_p \leq d_0$, the C-CFRTP part breaks by fracture mode 1 (Figure 3(a)). Only all the intra-layer cross-points fail. The tensile strength σ of C-CFRTP part can be calculated as Equation (1).

$$\sigma = \frac{n\sigma_c + \sigma_x}{n+1} \tag{1}$$

With the increasing of d_p, C-CFRTP part first breaks by fracture mode 2 (Figure 3(b)). The failure mainly occurs in all intra-layer cross-points and the matrix between adjacent intra-layer cross-points. The tensile strength σ of C-CFRTP part can be expressed as Equation (2).

$$\sigma = \frac{n}{n+1}\sigma_c + \frac{1}{n+1}\sigma_x + \frac{n-1}{n+1} \times \frac{d_p - d_0}{2b}\tau_p \tag{2}$$

where, τ_p is the in-plane shear strength of C-CFRTP part.

Then the continuous increase of d_p results that the shear force transmitted by the matrix is greater than the force caused by the reduced strength at the cross-points area. The fracture mode of C-CFRTP part converts to fracture mode 3 (Figure 3(c)). The tensile strength σ of C-CFRTP part reaches its maximum value and remains constant.

$$\sigma = \frac{1}{n+1}\sigma_c + \frac{n}{n+1}\sigma_x \tag{3}$$

Therefore, the variation of tensile strength σ for C-CFRTP part with the distance between adjacent intra-layer cross-points d_p is shown as in Equation (4).

$$\sigma = \begin{cases} \frac{n}{n+1}\sigma_c + \frac{1}{n+1}\sigma_x & 0 \le d_p \le d_0 \\ \min\left(\frac{n}{n+1}\sigma_c + \frac{1}{n+1}\sigma_x + \frac{n-1}{n+1} \times \frac{d_p - d_0}{2b}\tau_p, \frac{1}{n+1}\sigma_c + \frac{n}{n+1}\sigma_x\right) & d_p > d_0 \end{cases} \tag{4}$$

The tensile strength of C-CFRTP part σ with different distributions of inter-layer cross-points can be obtained by the same analysis method, as shown in Equation (5). It is worth emphasizing that the pores between inter-layer cross-points have little effect on interlayer bonding because of the large bonding area between layers. The fracture mode 2 (Figure 3(b)) will occur as long as the distance between the adjacent inter-layer cross-points (d_i) is not 0.

$$\sigma = \begin{cases} \sigma_c & d_i = 0 \\ \min\left(\sigma_c + \frac{m-1}{m} \times \frac{d_i}{h}\tau_i, \frac{1}{m}\sigma_c + \frac{m-1}{m}\sigma_x\right) & d_i > 0 \end{cases} \tag{5}$$

where, m is the number of inter-layer cross-points and τ_i is the interlaminar shear strength of C-CFRTP part.

Equation (4) and Equation (5) indicate the relation between cross-points distribution and tensile performance.

3 EXPERIMENTAL CONDITIONS

3.1 Material and experimental set-up

The PLA (polylactic acid) filament with 1.75 mm in diameter and the continuous carbon fiber bundle (T300-10000) were used in this paper to print the C-CFRTP specimens. All the C-CFRTP specimens containing these two materials were fabricated using the experimental set-up, as shown in Figure 5. It mainly included a nozzle structure, a printing platform, and a control system.

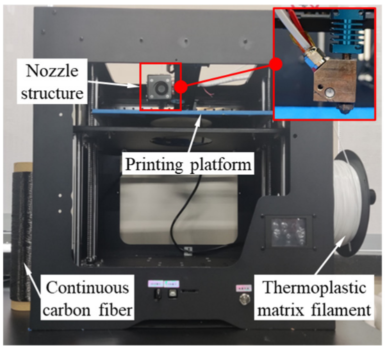

Figure 5: The 3D printer for C-CFRTP parts.

To verify the relation between cross-points distribution and tensile performance, the C-CFRTP specimens were printed by different cross-points distribution trajectories. The details distribution of cross-points is illustrated in Table 1. The length of the cross-point area along the fiber direction was 3mm. The printing trajectories shown in Figure 6 were used to fabricate the C-CFRTP specimens for measuring the tensile strength of fibers with non-cross-points σ_x and the tensile strength of fibers at cross-points σ_c, respectively. The main dimensions of the specimens used to measure tensile strength are listed in Table 2. Besides, a good combination of the process parameters is of great significance for higher tensile strength. The process parameter settings remain constant, as shown in Table 3. The impact of process parameters on tensile strength can be excluded. The cross-points distribution of was optimized based on this relation. Then the trajectory with the optimal and non-optimal distribution of cross-points were used to fabricate the C-CFRTP specimens, as shown in Table 4.

Specimen Number	d_p (mm)	d_i (mm)
1	0, 1, 2, 3, 4, 5, 6, 7, 8, 9, 10, 11, 12, 13, 14, 15, 16	0
2	0	0, 1, 2, 3, 4, 5, 6, 7, 8,

Table 1: The details cross-points distribution in the double-curve connection trajectory.

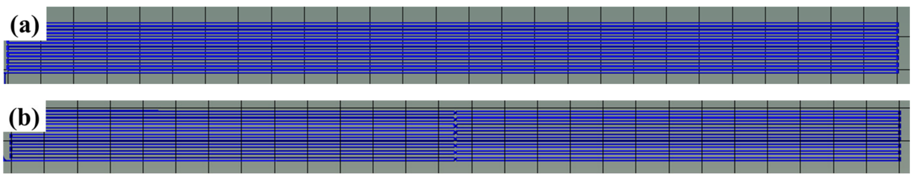

Figure 6: The printing trajectories to fabricate the specimens used to measure the tensile strength of (a) σ_x and (b) σ_c.

Length (mm)	Outer span (mm)	Width (mm)	Thickness (mm)	n	m
250	>136	16	1.2	7	4

Table 2: The main dimensions of tensile strength test specimens.

Printing speed (mm/s)	Nozzle temperature (°C)	Layer thickness (mm)	Hatch spacing (mm)
5	200	0.3	1

Table 3: Process parameters for fabricating C-CFRTP specimens.

Specimen Number	d_p (mm)	d_i (mm)	Is it optimal distribution
3	8	3	Y
4	0	0	N
5	13	0	N
6	0	6	N
7	The Zig-Zag trajectory (Figure 6(a))		

Table 4: The trajectory with the optimal and non-optimal distribution of cross-points.

3.2 Mechanical tests and observation of fracture forms

Tensile tests were conducted on a universal tester (WDW-100E, Wenteng Corp., Jinan, China) to evaluate the tensile strength of the FFF-fabricated C-CFRTP specimens. The tensile tests of specimens followed the ISO 527-5:2009 standard [20]. The tabs used in this measurement were the metal plates with 15mm×40mm×2mm. The test sample was fixed on the universal tester by grips. One grip was fixed while another moved with a 2 mm/min velocity. Moreover, the Keyence microscope (VHX-600E, Keyence Corp., Osaka, Japan) was used to observe the fracture mode of C-CFRTP specimens.

4 EXPERIMENTAL RESULTS AND MODEL VERIFICATION

4.1 Relation verification

The tensile test results showed that the tensile strength of fibers with non-cross-points σ_x and the tensile strength of fibers at cross-point σ_c were 320.17MPa and 256.76MPa, respectively. According to the measurement results of tensile tests, the relation between cross-points distribution and tensile performance are shown in Figure 7. The red lines in Figure 7 were the fitting results based on Equations (4) and (5). The experimental results were entirely consistent with the trend of theoretical analysis results.

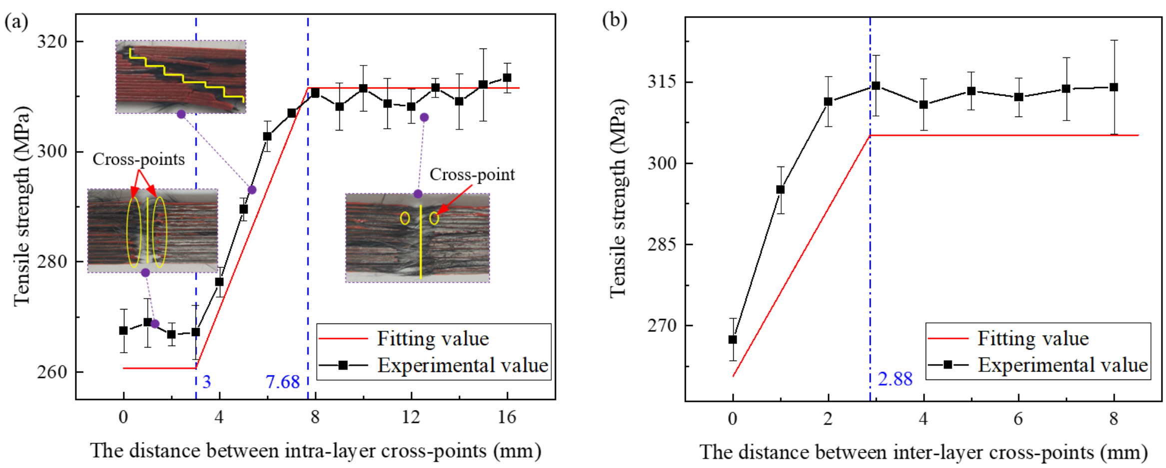

Figure 7: The relation between cross-points distribution and tensile performance: (a) intra-layer cross-points and (b) inter-layer cross-points.

As shown in Figure 7(a), the tensile strength of FFF-fabricated C-CFRTP specimens remained constant at about 267.43MPa when $d_p \leq$ 3mm. The specimens broke at the location where the intra-layer cross-points were concentrated. Only all intra-layer cross-points failed when broken, which was consistent with fracture mode 1. Then the tensile strength increased from about 276.36MPa to 310.71MPa, with the intra-layer cross-points distance ranging from 4mm to 8mm. When the C-CFRTP specimens broke, all intra-layer cross-points and the matrix between them failed, resulting in a stepped shape at the fracture location. The fracture in this case was consistent with fracture mode 2. Finally, the tensile strength reached a maximum value when the intra-layer cross-points distance was large enough ($d_p \geq$ 8mm). The tensile strength did not vary with the intra-layer cross-points distance. In this case, the C-CFRTP specimens broke in the form of fracture mode 3.

The relation between inter-layer cross-points distribution and tensile strength is shown in Figure 7(b). When d_i = 0mm, the specimens broke at the location where the inter-layer cross-points were concentrated. With the inter-layer cross-points distance ranging from 0mm to 3mm, the tensile strength increased rapidly from about 267.43MPa to 314.29MPa. Then the tensile strength reached a maximum value and remained constant. As the tensile strength gradually increased, the fracture mode of FFF-fabricated C-CFRTP specimens varied from mode 1 to mode 3.

It can be found from Figure 7 that the FFF-fabricated specimens, that failed by fracture mode 3, exhibited the higher tensile strength. Therefore, the optimization goal of cross-points distribution was to make the specimens fail by fracture mode 3.

4.2 Optimal distribution of cross-points

According to the relation between cross-points distribution and tensile performance, it can be found that the C-CFRTP specimens broke by fracture mode 3 when $d_p \geq$ 7.68mm and $d_i \geq$ 2.88mm. Therefore, the optimal cross-points distribution strategy was obtained, namely d_p = 8mm and d_i = 3mm. Then the tensile tests of C-CFRTP specimens printed by the trajectory with the optimal and non-optimal cross-points distribution were conducted. The test results indicate in Figure 8. The specimens printed by the optimal cross-points distribution trajectory (specimen number 3) exhibited a better tensile strength (320.86MPa), which was equal to the tensile strength of specimens printed by the Zig-Zag trajectory (specimen number 7). Compared with the specimens printed by the trajectory with non-optimal distribution (specimen number 4, 5 and 6), the tensile strength of specimen number 3 increased by about 19.97%, 2.96% and 2.78%, respectively. It can be seen that the optimal distribution of cross-points can eliminate the influence of the cross-points on the tensile strength of C-CFRTP specimens.

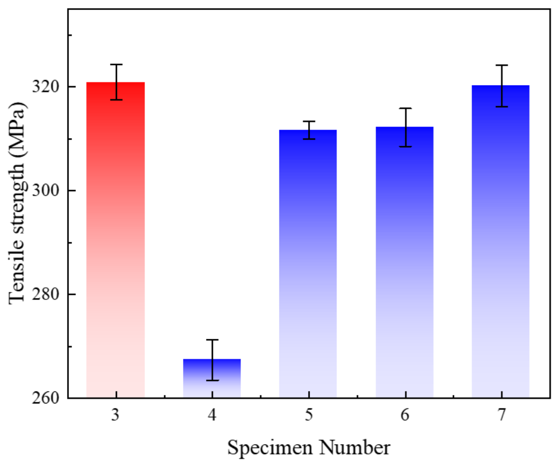

Figure 8: Comparison of tensile strength among the C-CFRTP specimens printed by the trajectory followed the optimal and non-optimal cross-points distribution.

5 CONCLUSIONS

In this paper, the relation between cross-points distribution and tensile performance was built and verified through theoretical analysis and tensile experiments. Based on that, the cross-points distribution was optimized for obtaining higher tensile strength, namely d_p = 8mm and d_i = 3mm. The optimal distribution can improve the tensile strength of C-CFRTP specimens to 320.86MPa, very close to the tensile strength of specimens printed by the non-cross-points trajectory (Zig-Zag trajectory).

The effect of distance between single-type cross-points on the tensile strength of C-CFRTP specimens was investigated in this paper. The tensile strength of C-CFRTP specimens with simultaneously distributed intra-layer cross-points and inter-layer cross-points should be further investigated to propose a more reasonable strategy for distributing intra-layer cross-points and inter-layer cross-points.

ACKNOWLEDGEMENTS

This work is supported by National Natural Science Foundation of China (Grant No. 52130506 and 52090053), Science and Technology Innovation Foundation of Dalian (Grant No. 2021RD08, 2022JJ12GX027).

REFERENCES

[1] A. M. Almushaikeh, S. O. Alaswad, M. S. Alsuhybani, B. M. AlOtaibi, I. M. Alarifi, N. B. Alqahtani, S. M. Aldosari, S. S. Alsaleh, A. S. Haidyrah, A. A. Alolyan, B. A. Alshammari, Manufacturing of carbon fiber reinforced thermoplastics and its recovery of carbon fiber: A review, *Polymer Testing,* 122, 2023, 108029.

[2] A. Uşun, R. Gümrük, The mechanical performance of the 3D printed composites produced with continuous carbon fiber reinforced filaments obtained via melt impregnation, *Additive Manufacturing,* 46, 2021, 102112.

[3] J. M. Chacón, M. A. Caminero, P. J. Núñez, E. García-Plaza, I. García-Moreno, J. M. Reverte, Additive manufacturing of continuous fiber reinforced thermoplastic composites using fused deposition modelling: Effect of process parameters on mechanical properties. *Composites Science and Technology,* 181, 2019, 107688.

[4] A. A. Stepashkin, D. I. Chukov, F. S. Senatov, A. I. Salimon , A. M. Korsunsky, S. D. Kaloshkin, 3D-printed PEEK-carbon fiber (CF) composites: Structure and thermal properties, *Composites Science and Technology,* 164, 2018, pp. 319-326.

[5] G. W. Melenka, B. K. O. Cheung, J. S. Schofield, M. R. Dawson, J. P. Carey, Evaluation and prediction of the tensile properties of continuous fiber-reinforced 3D printed structures, *Composite Structures,* 153, 2016, pp. 866-875.

[6] X. Tian, T. Liu, C. Yang, Q. Wang, D. Li, Interface and performance of 3D printed continuous carbon fiber reinforced PLA composites, *Composites Part A: Applied Science and Manufacturing,* 88, 2016, pp. 198-205.

[7] Q. Hu, Y. Duan, H. Zhang, D. Liu, B. Yan, F. Peng, Manufacturing and 3D printing of continuous carbon fiber prepreg filament, *Journal of Materials Science,* 53, 2018, pp. 1887-1898.

[8] N. Li, Y. Li, S. Liu, Rapid prototyping of continuous carbon fiber reinforced polylactic acid composites by 3D printing, *Journal of Materials Processing Technology,* 238, 2016, pp. 218-225.

[9] J. Qiao, Y. Li, L. Li, Ultrasound-assisted 3D printing of continuous fiber-reinforced thermoplastic (FRTP) composites, *Additive Manufacturing,* 30, 2019, 100926.

[10] Y. Huang, G. Fang, T. Zhang, C. C. L. Wang, Turning-angle optimized printing path of continuous carbon fiber for cellular structures, *Additive Manufacturing,* 68, 2023, 103510.

[11] R. Matsuzaki, M. Ueda, M. Namiki, T. Jeong, H. Asahara, K. Horiguchi, T. Nakamura, A. Todoroki, Y. Hirano, Three-dimensional printing of continuous-fiber composites by in-nozzle impregnation, *Scientific Reports,* 6, 2016, 23058.

[12] F. Wang, Z. Zhang, F. Ning, G. Wang, C. Dong, A mechanistic model for tensile property of continuous carbon fiber reinforced plastic composites built by fused filament fabrication, *Additive Manufacturing,* 32, 2020, 101102.
[13] F. V. D. Klift, Y. Koga, A. Todoroki, M. Ueda, Y. Hirano, R. Matsuzaki, 3D printing of continuous carbon fiber reinforced thermo-plastic (CFRTP) tensile test specimens, *Open Journal of Composite Materials,* 6, 2016, pp. 18-27.
[14] A. N. Dickso, J. N. Barry, K. A. McDonnell, D. P. Dowling, Fabrication of continuous carbon, glass and Kevlar fiber reinforced polymer composites using additive manufacturing, *Additive Manufacturing,* 16, 2017, pp. 146-152.
[15] C. Zeng, L. Liu, W. Bian, J. Leng , Y. Liu, Compression behavior and energy absorption of 3D printed continuous fiber reinforced composite honeycomb structures with shape memory effects, *Additive Manufacturing,* 38, 2021, 101842.
[16] S. Liu, Y. Li, N. Li, A novel free-hanging 3D printing method for continuous carbon fiber reinforced thermoplastic lattice truss core structures, *Materials and Design,* 137, 2018, pp. 235-244.
[17] N. Li a, G. Link, T. Wang, V. Ramopoulos, D. Neumaier, J. Hofele, M. Walter, J. Jelonnek, Path-designed 3D printing for topological optimized continuous carbon fiber reinforced composite structures, *Composites Part B: Engineering,* 182, 2020, 107612.
[18] Y. Huang, X. Tian, Z. Zheng, D. Li, A. V. Malakhov, A. N. Polilov, Multiscale concurrent design and 3D printing of continuous fiber reinforced thermoplastic composites with optimized fiber trajectory and topological structure, *Composite Structures,* 285, 2020, 115241.
[19] F. Wang, J. Zheng, G. Wang, D. Jiang, F. Ning, A novel printing strategy in additive manufacturing of continuous carbon fiber reinforced plastic composites, *Manufacturing Letters,* 27, 2021, pp. 72-77.
[20] ISO 527-5:2009, Plastics — Determination of tensile properties — Part 5: Test conditions for unidirectional fiber-reinforced plastic composites, International Organization for Standardization, https://www.iso.org/standard/52991.html